XL CILAMCE
IBERO-LATIN AMERICAN CONGRESS ON COMPUTATIONAL METHODS IN ENGINEERING
NOVEMBER 11-14, 2019
Praiamar Natal Hotel & Convention
Natal, RN-BRAZIL

COMPRESSION TESTS AND ANALYSIS OF BUILT-UP COLD-FORMED STEEL COLUMNS

Cristiane C.D.O. Bastos
Eduardo M. Batista
cdaemon@coc.ufrj.br
batista@coc.ufrj.br
Affiliation
Programa de Engenharia Civil, COPPE/UFRJ, Av. Horário Macedo, 2030, CT, Sala I 216, Cidade Universitária, 21941-594, Rio de Janeiro/RJ, Brasil

Abstract.

The present article includes the results of the structural stability of laced built-up cold-formed steel (CFS) columns, subjected to axial compression. The objective is to analyze the behavior of these spatial laced columns through full scale experimental tests, in which the collapse is caused by the interaction between local and global buckling in the compressed chord members. The spatial columns, composed of four plane-trussed members designed with lipped channel CFS and fully connected with self-drilling screws, were tested with 12200 and 16200mm length, 0.8 or 1.25mm plate thickness. In addition to these tests, it was also carried out experimental tests of columns´ chord members to obtain the collapse loads and comparison with the analytical DSM equations (direct strength method). The tested chord members were of 480mm length, double 88x86x40x42x12mm lipped channel cross-section and 0.8mm thickness. The results showed that the DSM can be applied to obtain the collapse loads of the chord built-up members, composed of two lipped channels connected with self-drilling screws. Two analytical methods were applied to obtain global buckling load of the special laced column and compared with numerical results. The obtained results indicated that critical buckling load may be accessed with the help of available analytical equations. The final results of the investigation indicate the adopted methodology, including the column global buckling nonlinear behavior combined with the collapse mode of the double lipped channel CFS chord members connected by self-drilling screws, is able to be applied for regular structural design of the CFS spatial trussed arrangement.

Keywords: Laced built-up columns, Cold-formed steel structures, Buckling, Elastic critical load, Column strength.

1 Introduction

Spatial laced columns composed of steel cold-formed steel members (CFS) are investigated in the present research, with the four chords connected with diagonal and bracing elements, conducting to trussed-type structural behavior. Hashemi and Jafari [1], Bonab *et al.* [2], Kalochairetis *et al.* [3], Hashemi and Bonab [4], have investigated the elastic critical load and strength of laced (or batten) columns through laboratory tests, but in all cases there were only two hot rolled chord members, connected by lacing bars. Dabaon et al. [5] presented an experimental investigation of built-up battened columns composed of two CFS channels placed back-to-back at varied spacing of intersection. Generally, it is shown that Eurocode EC3 [6] and AISI S-100 [7] specifications were unconservative for the built-up cold-formed steel section battened columns failing mainly by local buckling, while the specifications were conservative for the built-up columns failing mainly by elastic flexural buckling. El Aghoury *et al.* [8] presented the results of series of compression tests on battened columns that were composed of four equal slender angles. They concluded that interaction of torsional and flexural buckling modes reduced the column strength, and the columns composed of slender angles were very sensitive to geometric imperfections. Dar *et al.* [9] tested built-up columns fabricated using four CFS angle sections connected by single lacing systems. At this article, Eurocode EC3 [6] and AISI S-100 [7] provisions were considered inadequate for the prediction of design axial strengths of built-up laced CFS columns.

The behavior of a laced built-up column depends on its bending and shear stiffness, as well as on the connections stiffness. The effect of shear deformations may cause distortion of laced panels. Engesser [10] was the first to consider the shear deformation effect on the elastic critical load of columns. Bleich [11], Timoshenko and Gere [12], and several other researchers followed the original findings of Engesser, such as: Gjelsvik [13], Paul [14], Aslani and Goel [15] and Razdolsky [16-20].

The main objective of this article is to present the results of full-scale experimental tests carried out in spatial laced built-up columns, designed with lipped channel cold-formed steel members. Four spatial laced columns were tested, with 12200 and 16200mm length, 0.8 and 1.25mm plate thickness, and 400x400mm cross-section shown in Fig. 1(a). For the built-up column as a whole, elastic buckling and nonlinear FEM analyses were performed, with 3D bar elements. Two analytical methods were applied to obtain the global buckling load including shear effect, for pin-ended condition: Timoshenko [12] and Eurocode 3 [21].

Besides the effect of shear deformations, another issue that distinguishes the behavior of these columns from other structural systems, is the interaction between local and global buckling modes. As the collapse of the built-up laced columns, in the case of this study, is recognized when one of the longitudinal members (chords) reaches its axial compression capacity, it is necessary to know the compressive strength of the laced columns´ chords. In the case of this research, the laced columns´ chords were composed of two lipped channel members connected with self-drilling screws. The main design standards and specifications do not present methods for designing this type of cold-formed steel built-up section. As the DSM (Direct Strength Method) does not cover this type of built-up section used as chords in laced columns, to check the applicability of DSM, it was conducted experimental analysis of built-up cold-formed steel lipped channel stub columns, submitted to axial compression. The laced column longitudinal members (chords) were previously analyzed by the generalized beam theory (GBT), in order to identify its buckling loads and modes, and the analytical collapse load was obtained using DSM to compare with experimental results.

2 Laced built-up columns description

All tested columns have the same 400x400mm cross-section shown in Fig.1(a). The laced column chords shown in Fig.(c) were composed of two lipped channel members connected with 4.8mm diameter self-drilling screws spaced at each 220mm. Chords, diagonals and bracings are composed of

lipped channel CFS with the measured dimensions (average) of single lipped channel cross-section 88x86x40x42x12mm in Fig. 1(b). In order to evaluate the effect of global buckling, two lengths of columns were tested: 12200 and 16200mm, as shown in Table 1. Laced columns were manufactured with two steel plate thicknesses, for each column length: 0.8 or 1.25mm. The laced columns were tested in horizontal position, as illustrated in Fig, 2.

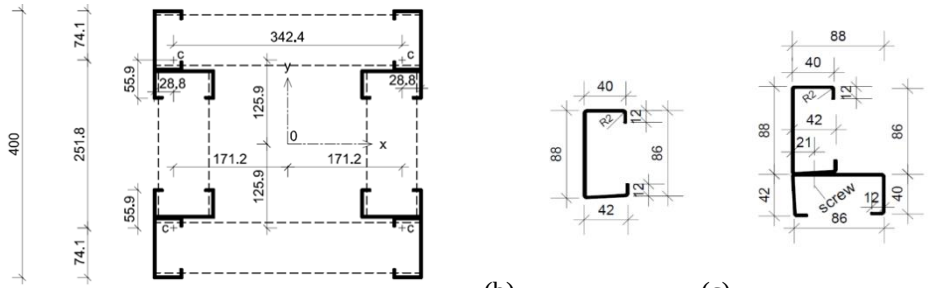

Figure 1. (a) Four chords laced built-up column cross-section (centroid of each chord is indicated with "+C"); (b) single lipped channel 88x86x40x42x12mm; (c) chords 2U88x86x40x42x12mm.

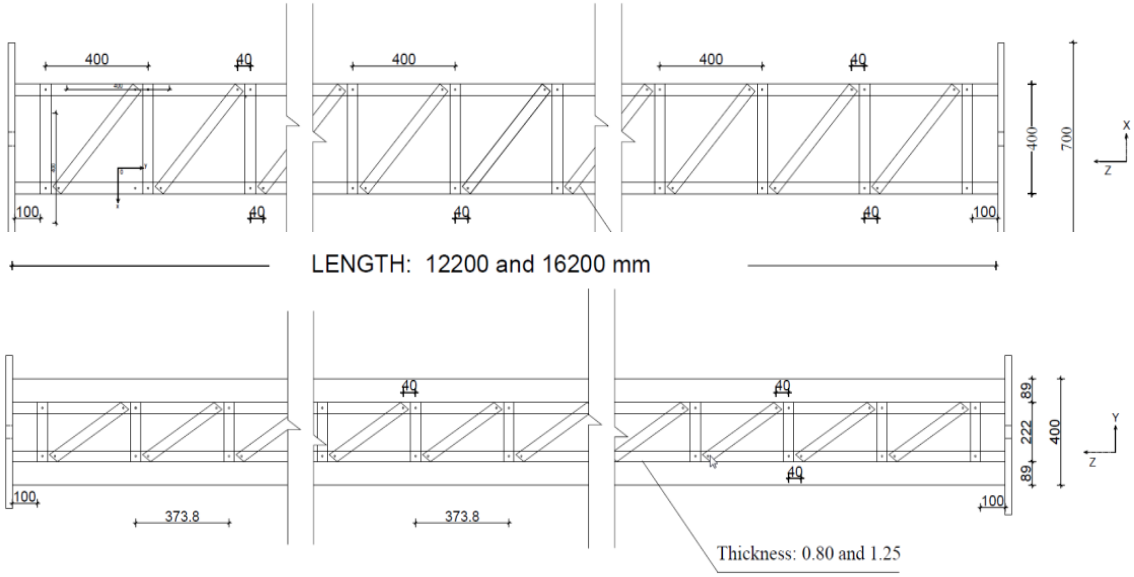

Figure 2. Lateral views of the laced built-up column placed in horizontal position for the test.

All diagonals and bracings of the built-up laced columns were connected to the chords with self-drilling screws, as shown in Fig.3. It can be observed that the chord's edge stiffeners have been cut off in the region of the arrival of diagonals and bracings, in order to enable connection. This type of connection, although practical, results in discontinuity of the cross-section of the chords, which may cause loss of loading capacity in this region. In addition, the exclusion of the cross-section edge stiffeners, even in a limited region, may originate increasing effect of the local buckling.

A total number of four spatial laced built-up columns, designed with lipped channel CFS, have been tested at the Structures Laboratory of COPPE, at the Federal University of Rio de Janeiro. Table 1 shows the columns IDs.

Table 1. Built-up laced column IDs.

Column ID	L (mm)	CFS
T12x0.8	12200	U88x86x40x42x12mm lipped channel CFS, t=0.8mm
T12x1.25	12200	U88x86x40x42x12mm lipped channel CFS, t=1.25mm
T16x0.8	16200	U88x86x40x42x12mm lipped channel CFS, t=0.8mm
T16x1.25	16200	U88x86x40x42x12mm lipped channel CFS, t=1.25mm

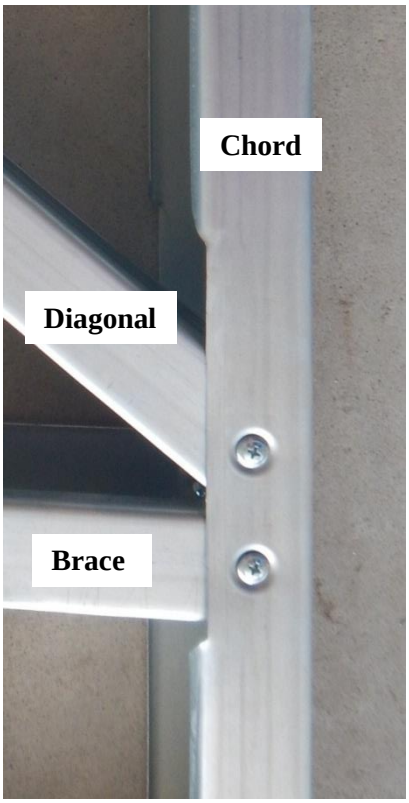

Figure 3. Lipped channel CFS bracing and diagonal connected with self-drilling screws (note the cut off region of edge stiffeners of the chord member).

3 Material properties

The laced columns were manufactured with structural steel (commercial identification ZAR345) with nominal yield stress f_y=345MPa. The steel mechanical properties were measured through standard tensile tests of 14 coupons extracted from the chord members (7 coupons for each thickness). The geometry of the coupons and the testing procedure were based on the guidance provided by ABNT ISO 6892 standard [22]. The average result of yield stress f_y, ultimate stress f_u, Young modulus E and residual strain after failure ε_r are given in Table 2.

Table 2. Average results of the standard tensile tests.

Thickness t (mm)	Yield Stress f_y (MPa)	Ultimate Stress f_u (MPa)	Young Modulus E (GPa)	ε_r %
0.8	370	477	198	20
1.25	375	479	215	18

4 Analysis of built-up chord member

The direct strength method (DSM) proposed by Schafer and Peköz [23] and considered in the North American standard AISI [7] was included in the Brazilian code ABNT NBR14762 [24], Annex C, for the design of cold-formed steel structural members. However, the DSM does not cover the design of built-up members, as is the case of the chords of the investigated laced column.

Research conducted by Fratamico *et al.* [25] indicated that composite action could develop in built-up sections, with axial compression and bending behavior capacity higher than the sum of the individual sections. Liu and Zhou [26] tested screw-connected T-section columns with the help of three lipped channel sections, for three different lengths. Zhang and Young [27-28] studied the

pertinence of the DSM for built-up open CFS members under axial compression, by comparing the results of a FEM parametric study with the experimental results of axial compression tests on I-shaped, open-section cold-formed steel with edge and web stiffeners. Based on rational buckling analysis, it was concluded that the current DSM could be used for the design of built-up open CFS columns. Liao *et al.* [29] studied multi-limb, built-up cold-formed steel stub columns with three different section forms and observed that the screw spacing has little effect on local and distortional buckling capacities and ultimate loads. Young and Chen [30] also conducted experiments on built-up CFS closed sections with intermediate stiffeners, with fixed-ended columns and different lengths. The authors concluded that DSM using a single section to obtain the local and distortional elastic buckling stresses is generally conservative and reliable, as composite action was not significant during tests.

The present study adopted the DSM to obtain the strength of the laced column longitudinal members (chords), composed of two lipped channel members as shown in Fig. 1(c). At item 4.2 will be presented the experimental analysis of a built-up cold-formed steel lipped channel stub column submitted to axial compression and a comparison between experimental and theoretical results, to check the applicability of DSM, as the method does not cover this type of built-up section used in laced columns. The Young modulus was assumed as E=198 and 215GPa, respectively for 0.8 and 1.25mm steel plates, according with standard tensile test results of specimens obtained from the laced columns (Table 2). Poisson ration is admitted as ν=0.3.

4.1 Elastic buckling analysis of the chord member

The analysis of the buckling modes and the corresponding critical buckling load P_{cr} is the first step for the design calculation using the DSM. Buckling analysis was performed taking into account pined-pined and free warping end condition, with the help of: (i) finite strip method (FSM), (ii) generalized beam theory (GBT) and (iii) shell finite element method (FEM). At this item, the actual screws connection condition between the CFS members was admitted as fully effective and transformed in double thickness ($2t$) plate element. Both lipped and unstiffened channel CFS chord member were considered, with 0.8 and 1.25mm thick steel plates as shown in Fig. 4.

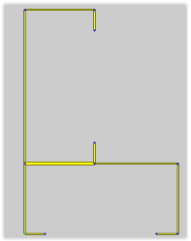

(a) Lipped channel 89x41x12mm

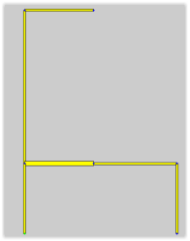

(b) Unstiffened channel 89x41mm

Figure 4. Chord built-up CFS for buckling analysis.

4.1.1 Finite strip method results

Software CUFSM [31], based on the finite strip method, was applied to obtain the buckling modes and corresponding elastic buckling loads of the chord member. The signature curve of double lipped channel U89x41x12x0.8mm is shown in Fig. 5.

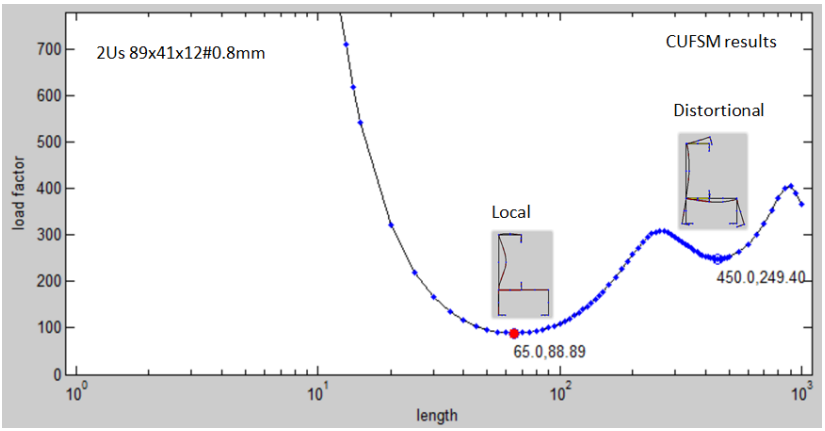

Figure 5. CUFSM results: buckling signature curve (σ_{critL} (MPa) x L (mm)) for built up lipped channel CFS 2Us 89x41x12x0.8mm.

4.1.2 Generalized beam theory (GBT) results

Stability analysis of thin-walled members may also be performed using GBT. Software GBTUL [32] was applied to obtain the buckling modes and corresponding elastic buckling loads of the chord member. The result of the analysis of double lipped channel U89x41x12x0.8mm is shown in Fig. 6.

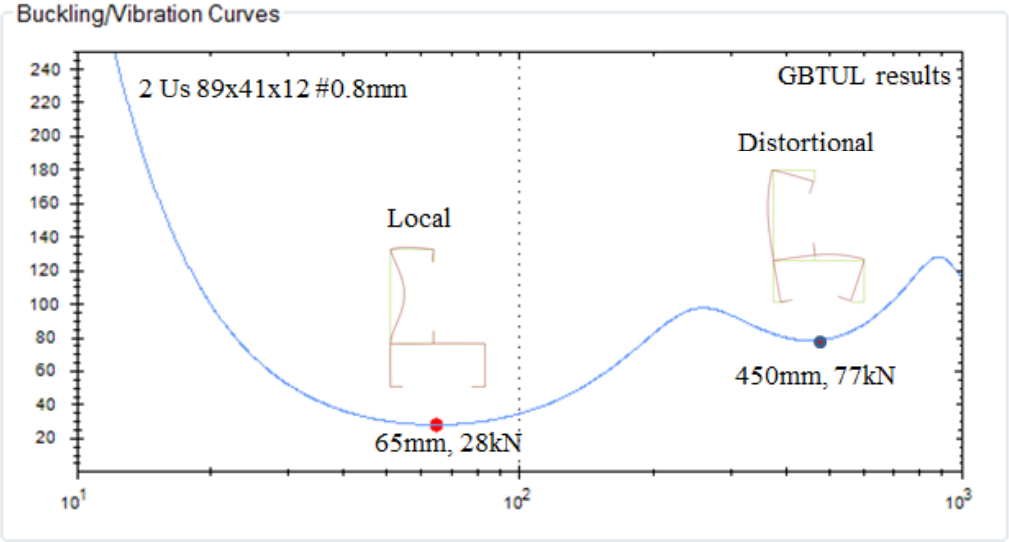

Figure 6. GBTUL results: buckling signature curve (P_{critL} (kN) x L (mm)) for built up lipped channel CFS 2Us 89x41x12x0.8mm.

4.1.3 Shell finite element method (SFEM) results

A mid-surface FEM model was developed and performed with shell finite element SHELL181 from the general finite element method package ANSYS R15.0 [33]. The model included mesh geometry with 5mm or 10mm size elements, showing accurate convergence between the obtained results.

The end support conditions were locally and globally pinned, free warping and twist prevented. This simply supported end condition was modeled by imposing null transversal displacements at all section nodes (axis x and y in Fig. 7). The axial displacement (axis z) was restricted at one mid-span node, in order to prevent rigid-body motion.

The chord member was modeled with length L corresponding to four local buckling semi waves (L=260mm for 2Us lipped channel 89x41x12mm and L=400mm for 2U unstiffened channel

89x41mm). Uniformly distributed compressive loading was applied at both end sections. The result of the analysis of the built-up lipped channel member is shown in Fig. 7.

The elastic buckling loads P_{crL} from the buckling analysis methods displayed in Table 3 shows quite accurate comparison. The ratio between critical buckling loads related to SFEM results are additionally indicated in Table 3 (inside parenthesis), from which it can be observed the larger difference obtained between FEM and CUFSM/GBTUL (approximately 8% difference). The critical buckling mode is local, developed in the web element as clearly observed in Figs. 5, 6 and 7.

Table 3. Results of the local buckling critical stress σ_{critL} and axial compressive load P_{crL}. The ratio between CUFSM or GBTUL results related to SFEM ones are included inside parenthesis.

		CUFSM		GBTUL		SFEM (10mm mesh)	
CFS (mm)	Area (mm^2)	σ_{critL} (MPa)	P_{crL} (kN)	σ_{critL} (MPa)	P_{crL} (kN)	σ_{critL} (MPa)	P_{crL} (kN)
2U89x41x12x0.8	309	90	28 (1.08)	90	28 (1.08)	83	26
2U89x41x0.8	271	57	15 (1.08)	57	15 (1.08)	52	14
2U89x41x12x1.25	480	240	115 (1.05)	241	115 (1.05)	229	110
2U 89x4x1.25	420	153	65 (1.06)	153	65 (1.06)	144	60

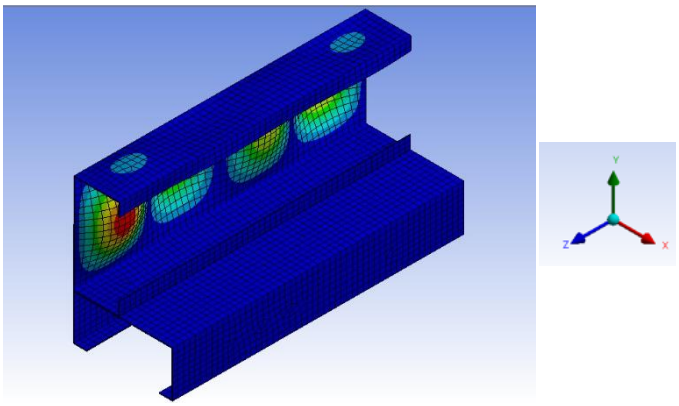

Figure 7. SFEM analysis result: local buckling mode for built up lipped channel CFS 2Us 89x41x12x0.8mm (5mm mesh).

4.2 Experimental analysis of built-up chord member

The experimental program included full-scale tests carried out on built-up cold-formed steel stub columns, composed of double lipped channels connected with 4.8mm diameter self-drilling screws, as shown on Fig. 1c). The tested columns are 480mm in length and 0.8mm thickness. Different arrangements of screws were tested, with two, three, four and five screws, as shown on Figure 8.

A total number of eight built-up columns were tested at the Structures and Material Laboratory of COPPE, at the Federal University of Rio de Janeiro. The built-up columns were previously prepared with 9mm plates Tig-welded at both extremities. Table 4 shows the columns IDs.

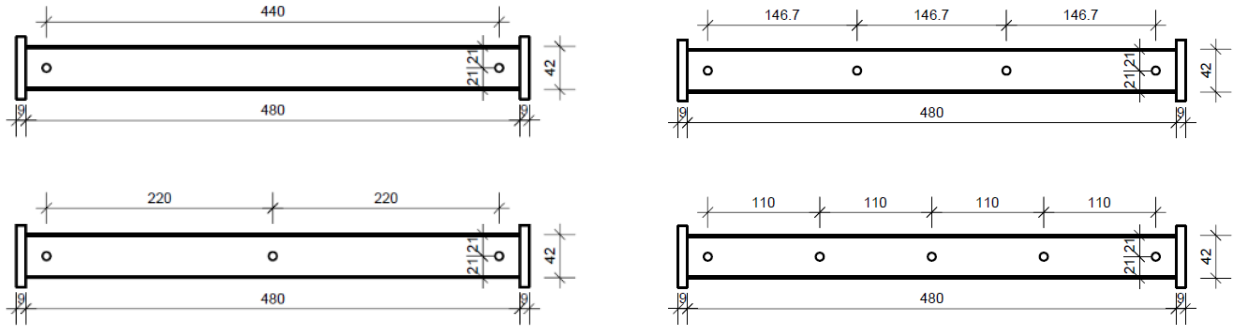

Figure 8. Tested built-up arrangements, with, 2, 3, 4 and 5 self-drilling 4.8mm screws.

Table 4. Built-up columns IDs: 2 lipped channel CFS 88x86x40x42x12mm, t=0.8mm.

Column ID	Number of self-drilling 4.8mm screws
CP1-03, CP2-13	2
CP3-14, CP4-16	3
CP5-09, CP6-18	4
CP7-17, CP8-10	5

4.2.1 Testing procedure and measuring devices

The built-up columns were tested in a displacement control condition, with compression load applied by a servo controlled hydraulic actuator. The actuator was placed in a rigid frame, as shown in Fig. 9(a), programed at a 0.004mm/s rate smooth displacement control. The end condition for the axial compression test was rigid type for flexural rotations (constrained ends), as confirmed by the recorded experimental measurements of test set-up templates, described further on. The identification of bottom and top templates are, respectively, Template 1 and 2.

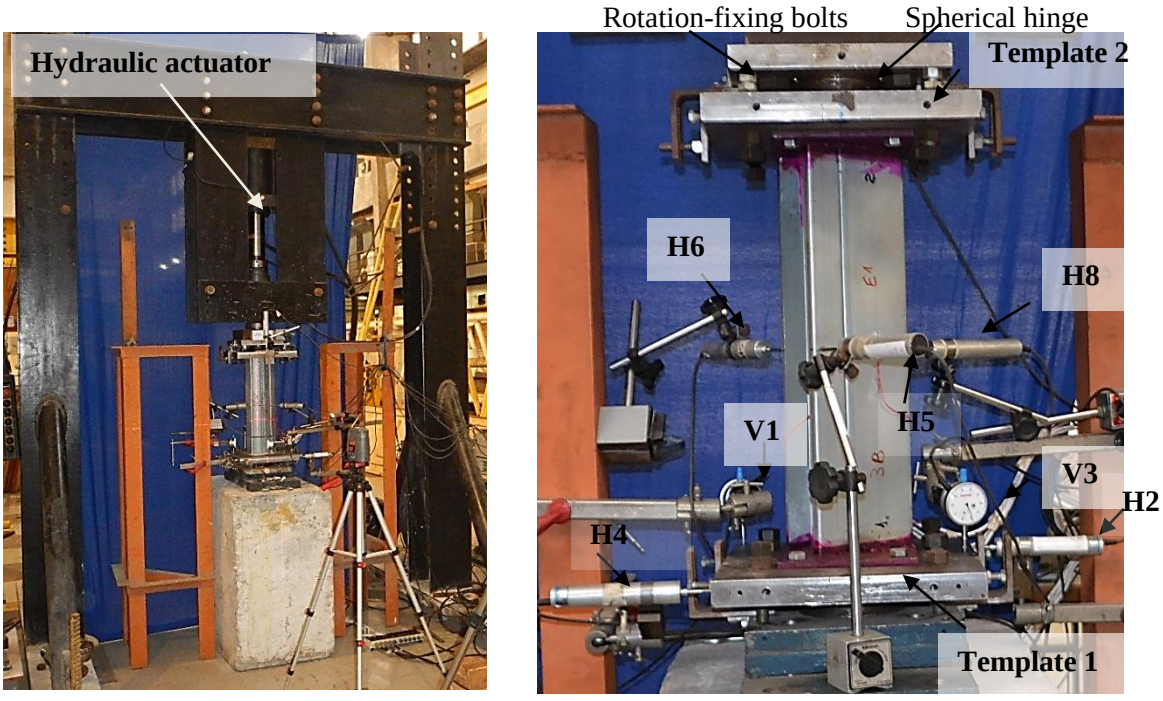

(a) (b)

Figure 9. Experimental set-up: (a) Testing frame arrangement; (b) displacement transducers DTs for (i) vertical and horizontal measurements at bottom template 1 (V1 and V3, H2 and H4)) and (ii) at the column mid-length (H5, H6 and H8 – see Fig. 10(a)).

Displacement transducers (DTs H5, H6 and H8) were applied for flange deflection measurements at the mid-length of the column, as shown in Fig. 9. Additional DTs were placed to follow displacements and rotations at the top template 2 (V7) and bottom template 1 (V1, V3, H2 and H4). These measurements allow end condition control, in order to confirm the constrained condition at the templates, which must be assured by the rotation-fixing bolts indicated in Fig. 9(b). Fig. 9(b) shows the DTs placed at the test machine bottom template 1 (V1, H2, V3 and H4) and at column mid-length (H5, H6 and H8). Longitudinal strain gages were placed externally and internally in the webs of both lipped channels, at the mid-length of the column, thus performing two couples of strain gages addressed to record the onset of local buckling deformation. Figure 10(b) displays the distribution of strain gages.

a) b)

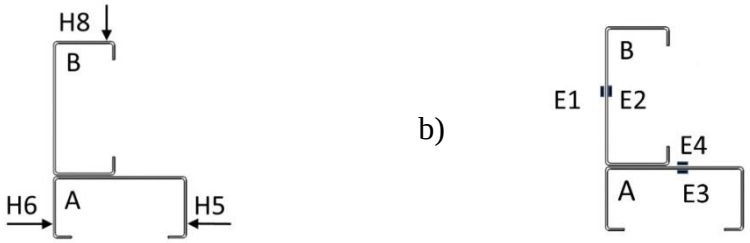

Figure 10. Measurement devices placed at the mid-length section of the columns: a) displacement transducers DTs H5, H6 and H8, b) longitudinal couples of strain gages E1-E2 and E3-E4.

The process adopted for centering the specimens in the testing set up followed a graphic scheme. This method consisted of stamping the cross-section of the columns on graph paper (for both ends). The geometric characteristics were computed through the actual cross-section geometry drawn, including the position of the centroid. Next, the centroid of each section was marked over the original drawing, as well as the actual principal axis of inertia. The graph paper with the stamped cross-section was fixed over the end plates, coinciding its centroids, defining the TIG-welding position. Finally, the end plates of the column were bolted to the top and bottom templates. A laser level device was used to check column position and verticality.

4.2.2 Tests results

During the tests of the built-up columns, it was possible to observe (by naked eye) the development of the typical local buckling deformation mode along the webs of the members (A and B) before collapse. Although the web of member A was partially fixed to the flange of member B, local and distortional buckling deformation was clearly observed and measured, showing that the screw connection was not fully effective. Fig. 11(a) shows the local and distortional buckling semi-waves developed during the test for CP8-10. Table 5 describes the approximate position of the collapse mechanism for the tested built-up columns. Fig. 11(b) shows the collapse mechanism for CP4-16.

Table 5. Registered position of the collapse mechanisms.

Column ID	Member A	Member B
CP1-03	quarter-length	mid-length
CP2-13	quarter-length	mid-length
CP3-14	quarter-length	quarter-length
CP4-16	mid-length	mid-length
CP5-09	mid-length	top (end 2)
CP6-18	top (end 2)	mid-length
CP7-17	top (end 2)	top (end 2)
CP8-10	bottom (end 1)	bottom (end 1)

The flanges of members A and B deformed inward (closing) during the tests, as may be seen in Fig.11(a) and b). Figure 12(a) shows the horizontal displacements recorded by DTs H5, H6 and H8 at the mid-length of column CP3-14, indicating the non-linear behavior for loads greater than 30kN. This

behavior was similar for all tested columns, indicating the presence of a distortional buckling. Experimental measurements from the DTs V1, H2, V3, H4 and V7, placed at bottom and top set-up templates, registered minor displacements (less than 0.6mm for vertical DTs and less than 0.05mm for horizontal DTs), confirming the constrained ends.

The mid-length longitudinal couples of strain gages registered linear (compression) behavior until the onset of local buckling. Figure 12(b) shows the strain gage results for the built-up column CP3-14, where near linear behavior can be observed until (approx.) 13kN applied load. The beginning of the local buckling effect was recorded for member B, in accordance with measurements of couple of strain gages E1/E2. The registered collapse load was 56kN.

Finally, Table 6 shows a summary of the results for the tested built-up columns, including the records of (i) the collapse load P_{uexp}, and (ii) the loading level (approx.) for which the onset of local buckling was identified P_{Lexp}, with the help of strain gage measurements.

a) 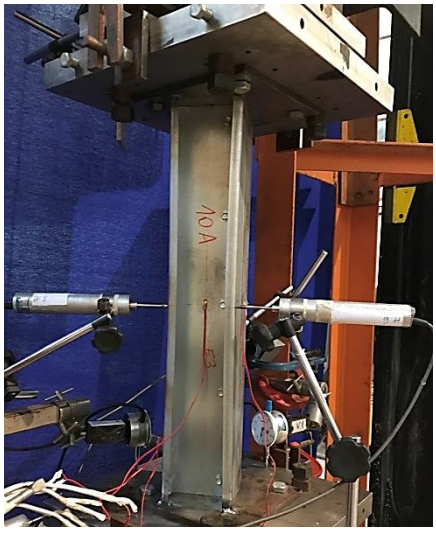 b) 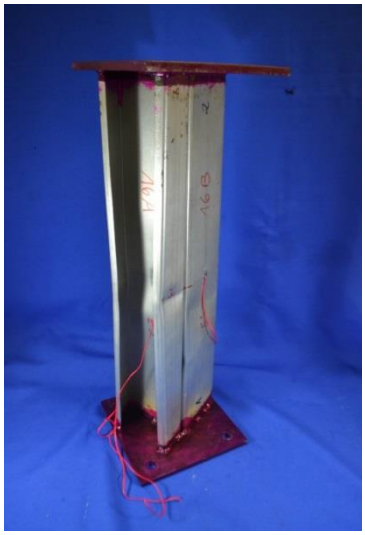

Figure 11. Test results of columns: (a) seven local buckling semi-waves in the web combined with single distortional buckling observed in member A of CP8-10; (b) Collapse mechanism of CP4-16: Mid-length combined local and distortional buckling for members A and B.

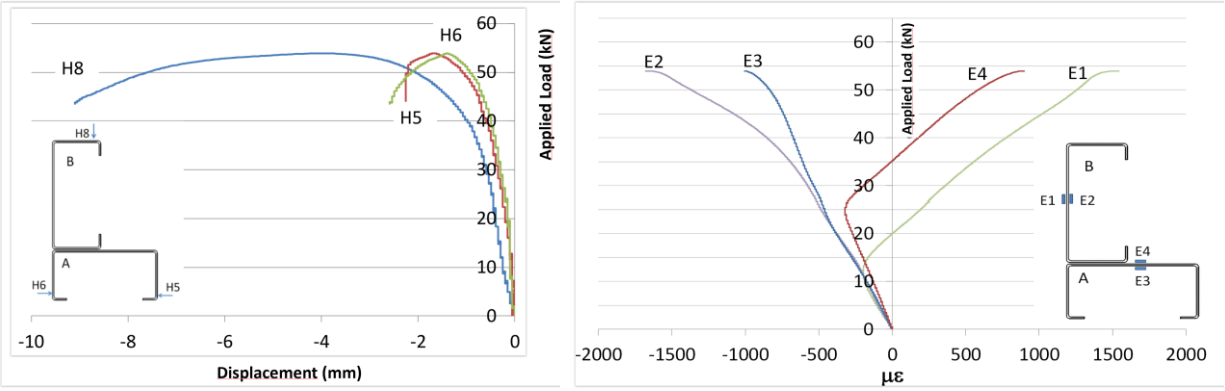

a) b)

Figure 12: a) Load vs. displacement recorded at the column mid-length for built-up column CP3-14; b) load vs. strain measurements (με) at mid-length section of the built-up column CP3-14.

Table 6. Experimental results of tested built-up columns.

Column ID	Number of screws	Collapse load P_{uexp} (kN)	Local buckling onset P_{Lexp} (kN)
CP1-03	2	53.90	11.00
CP2-13	2	55.40	13.00
CP3-14	3	56.05	13.00
CP4-16	3	55.25	13.00
CP5-09	4	56.30	16.00
CP6-18	4	54.55	15.00
CP7-17	5	55.60	15.00
CP8-10	5	53.70	23.00
Average		55.09	14.88
Standard deviation		0.96	3.64
Coef. of variation		1.7%	24.5%

As observed in the results of the tests, although improved results of the onset of the local buckling were recorded during the tests, especially for the case of 4 and 5 screw connections (see table 6), the ultimate load (column strength) was marginally affected. The explanation for this performance is the fact that the local buckling mode is mainly affected at the connected elements and develops almost freely in the other plate elements. This statement is confirmed by the fact that the experimentally observed local buckling shape, especially in the web element not restricted by the fasteners, strictly corresponds to the theoretical one computed for a single column member with the help of the generalized beam theory (seven local buckling semi-waves with 69mm length, see Fig.13(d)). The collapse load values (P_{uexp}) were very similar between the tested built-up columns, regardless of the number of screws adopted to connect members A and B. The average value was 55.1kN with negligible standard deviation.

4.2.3 Design Methods

Buckling analysis was performed taking into account a constrained ends condition (to simulate experimental conditions of item 4.2.1), using the generalized beam theory with the help of the GBTUL computational program (Bebiano *et al*., [32]). The actual screw connection condition between the CFS members was admitted as fully effective (fully-composite) and transformed into a double thickness ($2t$) plate element in the portion of contact between the web and flange of the element members A and B, respectively. In addition, a non-composite condition was admitted, considering the single section of members A and B, for comparison.

The analyses performed with GBTUL considered the actual dimensions of each specimen, with imperfections. Figure 13 shows, as an example, the GBTUL fully-composite section, with double thickness at the contact between the flange of member B with the web of member A. The Young modulus was assumed as E=198 GPa and the yield strength f_y=370MPa, according with standard tensile test results included in Table 2. Poisson ration is admitted as $\nu = 0.3$.

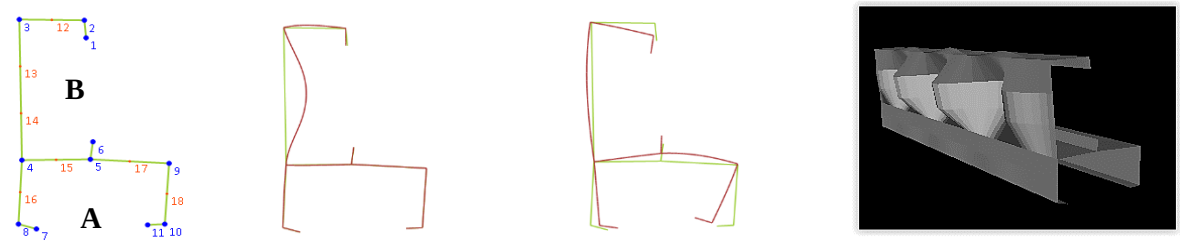

a) b) c) d)

Figure 13. (a) GBTUL fully-composite section (double thickness in the contact portion) and constrained ends condition (C-C); (b) local buckling deformation mode; (c) distortional buckling deformation mode; d) seven local buckling semi-waves along 480mm length.

Figure 14 shows the GBTUL non-composite section (members A and B computed separately). The deformation modes for local buckling are shown in Figures 13b) and 14b), and distortional buckling in Figures 13c) and 14c).

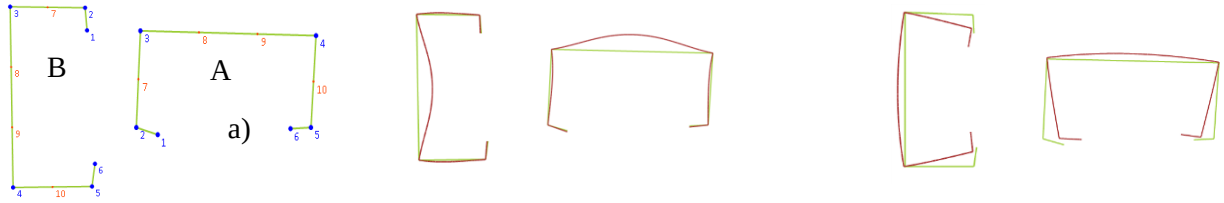

a) b) c)

Figure 14. (a) GBTUL non-composite section (members A and B); (b) local buckling deformation mode; c) distortional buckling deformation mode.

The DSM design rules for columns are described below, Eq. (1) to (6). The column strength (P_n) is taken as the lowest value provided by local-global LG buckling interaction (P_{nLG}) or the distortional buckling (P_{nD}). In the following equations, P_{crG} is the elastic global buckling load; P_{crL} is the elastic local buckling load and P_{crD} is the elastic distortional buckling load.

$$P_{nG} = \left(0.658^{\lambda_0^2}\right) A f_y \qquad \text{for } \lambda_0 \leq 1.5. \tag{1}$$

$$P_{nG} = \left(\frac{0.877}{\lambda_0^2}\right) A f_y \qquad \text{for } \lambda_0 > 1.5 \quad \text{where} \quad \lambda_0 = \left(\frac{A f_y}{P_{crG}}\right)^{0.5}. \tag{2}$$

$$P_{nLG} = P_{nG} \qquad \text{for } \lambda_L \leq 0.776. \tag{3}$$

$$P_{nLG} = \left(1 - \frac{0.15}{\lambda_L^{0.8}}\right) \frac{P_{nG}}{\lambda_L^{0.8}} \qquad \text{for } \lambda_L > 0.776 \quad \text{where} \quad \lambda_L = \left(\frac{P_{nG}}{P_{crL}}\right)^{0.5}. \tag{4}$$

$$P_{nD} = A f_y \qquad \text{for } \lambda_D \leq 0.561. \tag{5}$$

$$P_{nD} = \left(1 - \frac{0.25}{\lambda_D^{1.2}}\right) \frac{A f_y}{\lambda_D^{1.2}} \qquad \text{for } \lambda_D > 0.561 \text{ where} \quad \lambda_D = \left(\frac{A f_y}{P_{crD}}\right)^{0.5}. \tag{6}$$

The values of P_{crL} and P_{crD} were obtained from GBTUL considering a constrained-constrained (C-C) end condition to simulate experimental conditions of item 4.2.1.

From the experimental tests, it can be observed that members A and B developed a local buckling mode with seven semi-waves and distortional buckling modes with a single wave. The buckling modes were similar to the modes obtained from GBTUL for the non-composite section presented in Fig. 14. Figure 12(b) shows the local buckling in the web of member A started afterwards, with an approximate applied load of 21kN, registered by strain gage E4. Meanwhile, for member B, the on-set of local buckling was 13kN, registered by strain gage E1. The observed performance is explained by the web of member A, partially constrained by the flange of member B (observe Figs. 1(c) and 13).

As the local buckling was predominant (remember that global buckling is excluded in the present investigation), Table 7 shows the values of the local buckling critical load P_{crL}, for the non-composite section (member A and B) and fully-composite section (the lowest value obtained between the measured cross-section geometries of the column top and bottom ends). Table 7 shows also the collapse load P_{uth} obtained from DSM, for the non-composite section (A+B) and fully-composite section, as well as the ratio between them. The ratio fully/non-composite was 1.04 (average) for the collapse load P_{uth}. As the members A and B are connected with screws at discrete points, the actual condition may be considered in between the non-composite and fully-composite values.

Table 8 shows the experimental and DSM-based theoretical collapse loads for the tested built-up columns, considering non-composite and fully-composite, as well as the ratio between results. It can be observed that theoretical non-composite hypothesis is in very good agreement with the experimental collapse loads, with an average value of 55.1kN and insignificant standard deviation. These results are sustained by the evidence that the connection between member A and B was not fully effective, as observed during the test.

Table 7: Computed values for elastic local buckling P_{crL} and DSM-based collapse load P_{uth}.

	P_{crL} (kN) - GBTUL			P_{uth} (kN) - DSM		
Column ID	Member A	Member B	Fully composite	Non composite (A+B)	Fully composite	Fully / Non
CP1-03	12.60	12.35	28.05	54.98	57.63	1.05
CP2-13	12.99	12.78	28.67	55.70	58.09	1.04
CP3-14	12.68	12.57	27.91	55.01	57.04	1.04
CP4-16	12.52	12.06	27.77	55.09	57.95	1.05
CP5-09	12.68	12.83	27.71	55.44	57.56	1.04
CP6-18	12.60	12.92	27.50	55.08	57.44	1.04
CP7-17	12.45	12.95	27.21	55.00	56.85	1.03
CP8-10	12.38	12.66	27.22	54.74	56.82	1.04
Average	12.62	12.65	27.74	55.19	57.48	1.04
Standard deviation	0.29	0.24	0.66	0.50	0.76	0.01
Coef. of variation	2.3%	1.9%	2.4%	0.9%	1.3%	0.6%

Table 8: Comparison between experimental and theoretical loads of the built-up lipped channel columns, considering non-composite and fully-composite members.

	Experimental		Theoretical DSM strength P_{uth}			
Column ID	Number of screws	Collapse load P_{uexp}	Non composite (members A+B)	Experim./ Non –comp.	Fully composite	Experim./ Fully comp.
CP1-03	2	53.90	54.98	0.98	57.63	0.94
CP2-13	2	55.40	55.70	0.99	58.09	0.95
CP3-14	3	56.05	55.01	1.02	57.04	0.98
CP4-16	3	55.25	55.09	1.00	57.95	0.95
CP5-09	4	53.60	55.44	1.02	57.56	0.98
CP6-18	4	54.55	55.08	0.99	57.44	0.95
CP7-17	5	55.60	55.00	1.01	56.85	0.98
CP8-10	5	53.70	54.74	0.98	56.82	0.95
Average		55.09	55.19	1.00	57.48	0.96
Standard deviation		0.96	0.50	0.02	0.76	0.02
Coef. of variation		1.7%	0.9%	1.5%	1.3%	1.8%

The results indicated that the direct strength method (DSM) proposed by Schafer and Peköz (1998) is able to estimate the ultimate strength of this type of built-up lipped channel section. The better results of the computed column strength were obtained for the non-composite built-up channel CFS.

4.3 Laced columns chords members

Based on the experimental results of item 4.2, non-composite condition was admitted for the laced columns chords members, considering the single section (members computed isolated), with the dimensions of figure 1b), with 0.8 and 1.25mm thickness. Both lipped and unlipped channel CFS chord member were considered, due to localized suppression of edge stiffeners at the connections. The Young modulus was assumed as E=198 and 215GPa, respectively for 0.8 and 1.25mm steel plates, according with standard tensile test results of specimens obtained from the laced columns (table 2). Poisson ration is admitted as 0.3.

The GBTUL non-composite sections (members A and B) for lipped channel chord members, and the buckling modes, are illustrated in Fig. 14. The GBTUL non-composite sections for chord members without edge stiffeners (unlipped channels), and the buckling modes, are illustrated in Fig. 15. Table 9 presents the values of λ_L, P_{crL} , λ_D and P_{crD}, considering the lipped channel single U (member A, Figure 15) and the double U (member A + member B, Figure 14), for 0.8 and 1.25mm thickness. As the CPs are stub columns, the global buckling loads (P_{nG}) were much higher. According to Matsubara, Batista and Salles [34], for the case of CFS lipped channel columns with DL slenderness ratio ($R_{\lambda DL}=\lambda_D/\lambda_L$) less than 0.45, the local mode is predominant, and for $R_{\lambda DL}$ greater than 1.05, the distortional mode is predominant. Lipped channel columns with a slenderness ratio $R_{\lambda DL}$ ranging between 0.45 and 1.05 developed a local and distortional buckling mode interaction, LD. In the present case, the ratio

slenderness ratio was $R_{\lambda DL}$ = 0.36 for 0.8mm thickness, and 0.52 for 1.25mm thickness, indicating that local buckling was predominant for 0.8mm thickness and probable (weak) interaction between local and distortional modes for 1.25mm thickness.

Table 9 : Elastic buckling for chord members: local (λ_L, P_{crL}) and distortional (λ_D, P_{crD}).

CFS	P_{crL} (kN)	P_{crD} (kN)	λ_L	λ_D	λ_L / λ_D
Single U #0.8mm	13.4	105.6	2.06	0.73	0.36
Double U (2U) #0.8mm	28.7	226.8	1.99	0.71	0.36
Single U #1.25mm	55.1	207.1	1.28	0.66	0.52
Double U (2U) #1.25mm	118.3	456.8	1.24	0.63	0.51

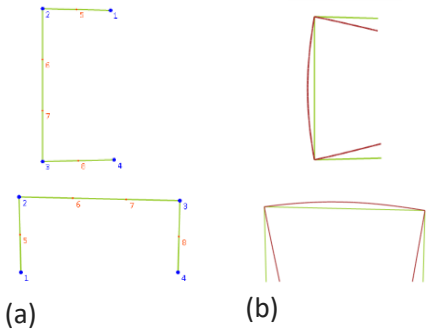

Figure 15: a) GBTUL non-composite section (members A and B) without edge stiffeners (unlipped channel); b) local buckling deformation mode.

As the local buckling was predominant in the present case, table 10 shows the values of P_{crL} for non-composite section, for single U. As the laced column has 400mm modulation (see Fig. 2), the compression strength of the chord was computed for constrained end condition and length L=400mm. Table 10 also presents the collapse load P_n obtained from DSM, for single U, for one chord (2U's) and for four chords (8U's). It was considered the measured yield stress from tensile tests f_y = 370 and 375MPa, for t=0.8 and 1.25mm respectively.

Table 10: DSM column strength of the built-up chord members with constrained end condition, length L=400mm, considering non-composite behavior.

Built-up CFS	Thickness *(mm)*	GBTUL *Single U* P_{critL}	DSM *Single U* P_n (kN)	*1 Chord* (2U's) P_{n2} (kN)	4 Chords (8U's) P_{n4} (kN)
Lipped channel U 88x86x42x40x12	0.80	13.4	28.8	57.5	230.1
Unlipped channel U 88x86x42x40	0.80	7.0	20.6	41.1	164.5
Lipped channel U 88x86x42x40x12	1.25	54.0	63.4	126.9	507.4
Unlipped channel U 88x86x42x40	1.25	26.8	44.9	89.8	359.0

5 Analysis of spatial laced columns

5.1 Elastic buckling analysis of laced columns

In order to evaluate the global buckling of laced columns, numerical model was developed with the help of the finite element method with beam elements (BFEM). For this, SAP2000 [35] computational program was achieved. The laced columns were taken as pined-pined and they were described by the centroid axis of the chords, as indicated in Fig. 1(a). The first two buckling modes are flexural buckling around X and Y axes, the third buckling mode is torsional and the fourth one is the second flexural buckling mode around X-axis. Buckling loads from numerical BFEM model are presented forward in the Table 12.

5.2 Experimental analysis of laced columns

The built-up laced columns were tested in horizontal position, with compression load applied by a servo controlled hydraulic actuator. The actuator was placed at one end of the column, as shown in Fig. 16, and a Dywidag steel rod crosses through the column length and is attached to a reaction stiff plate placed at the opposite end of the laced column. Loading condition was programed to smooth displacement control at 0.02mm/s rate.

The end condition for axial compression test was actually a semi-rigid type for flexural rotations (not perfect pined-pined). Rigid plate combined with spherical hinge was adopted at end section as shown in Fig. 16. Semi-rigid behavior was imposed, since the spherical hinge is not able to allow actual free rotations for low loading condition.

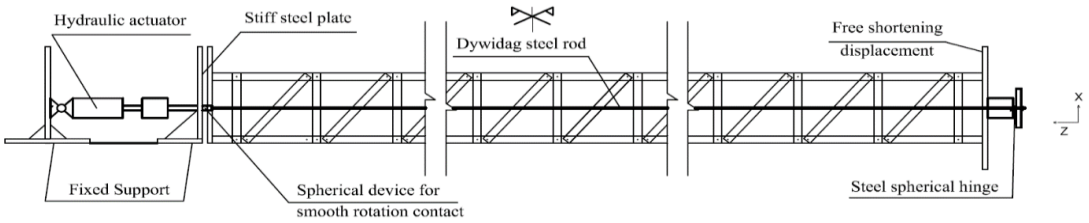

Figure 16: Load application schematic arrangement.

Displacement transducers (DT) were applied for minor and major axis deflection measurements, at mid-length and quarter-lengths of the column and close to the fixed end support. The minor inertia plane was placed in horizontal position for the tests.

The strain gauge distribution included four sensors at each column end, and at the mid-length, placed externally in the web element of the chords, addressed to record the onset of local buckling deformation.

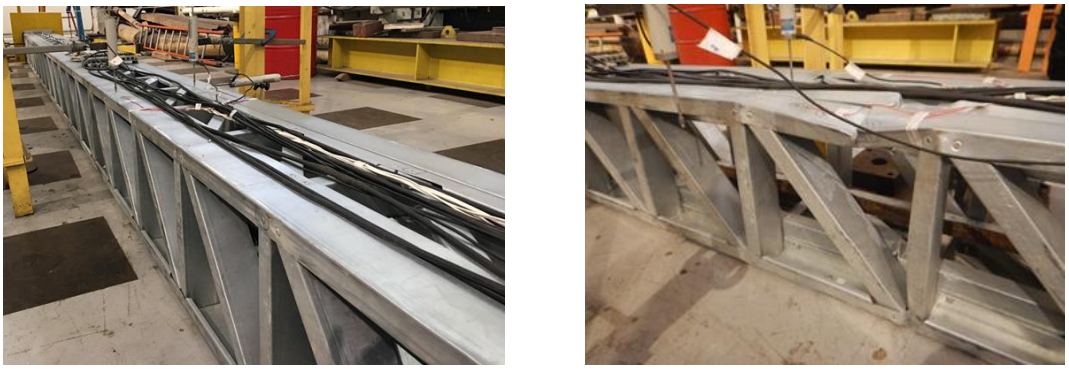

(a) (b)

Figure 17: Column T12x0.8, nominal length 12200mm: (a) Local buckling deformation along the chords during the test, (b) collapse mechanism at mid length.

During the tests of the laced columns, it was possible to observe the development of typical local buckling deformation mode along the webs of the chords before collapse. Although observed in almost all the tested columns, it was more visible for the case of 0.8mm thick built-up laced columns, due to more slender CFS. Figure 18(a) shows the local buckling mode developing along the chords. Laced columns with nominal lengths 12200 and 16200mm developed clear global buckling deformation with collapse mechanism at the mid length. It was possible to observe interaction between local (at the chord members) and flexural global buckling modes.

Figure 18 shows the horizontal displacements w recorded by displacement transducers at mid-length (DT-4H), quarter length (DTs 9H and 10H) and near fixed end (DT-2H) of column T12x1.25, indicating almost null flexural displacements until (aprox.) 110kN. As referred, the spherical hinges were not able to allow free rotations for low loading condition. Higher loading developed flexural buckling behavior which forced and liberated rotations at the ends of the laced column.

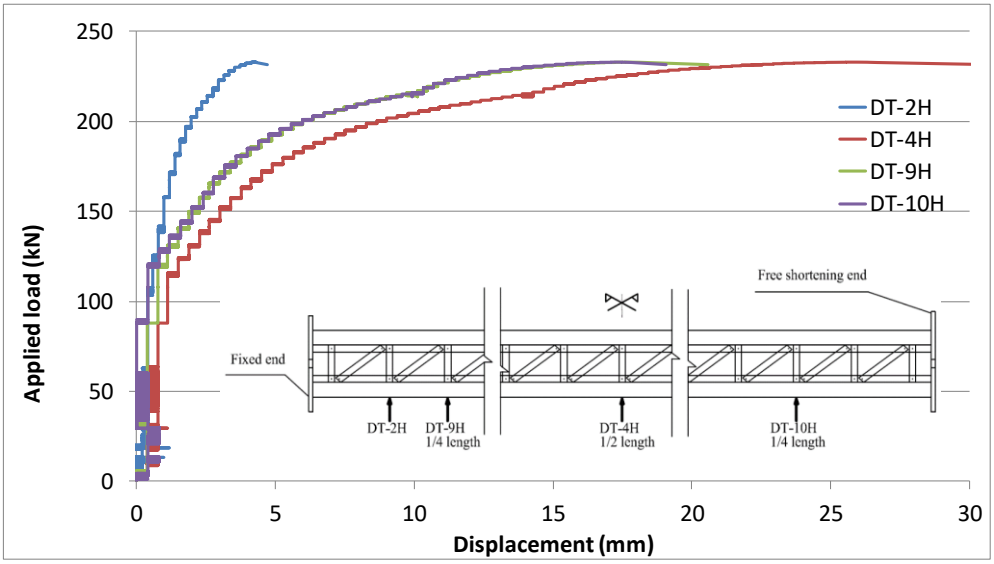

Figure 18. Experimental results of column T12x1.25: Load *vs*. horizontal displacement recorded at the column mid-length.

The strain gauges registered linear (compression) behavior until the onset of local buckling. Figure 19 shows the strain gauges results for the built-up laced column T12x1.25, where nearly linear behavior can be observed until (aprox.) 80kN applied load. The beginning of local buckling effect was recorded by strain gauge SG-10R. The registered collapse load was 233kN.

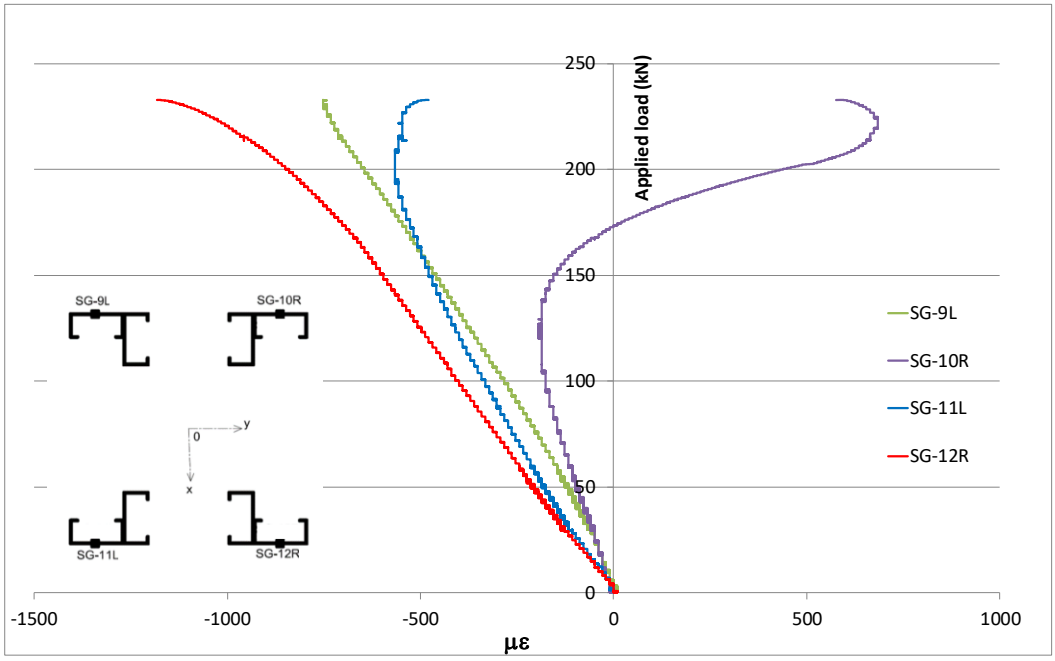

Figure 19. Load *vs*. strain measurements (με) at mid-length section of the laced column T12x1.25.

Finally, Table 11 shows a summary of the results for the tested built-up laced columns, including the records of (i) the collapse load (P_{uexp}), (ii) the mid-length flexural displacement at the collapse load level and (iii) the loading level for which the onset of local buckling was identified (with the help of strain gage measurements).

Table 11: Summary of the test results of the built-up laced columns.

Buit-up laced column	Collapse load P_{uexp} (kN)	Mid-length displacement (mm)	Local buckling load (kN)*
T12x1.25	233	31	80
T12x0.8	89	45	25
T16x1.25	196	71	85
T16x0.8	85	59	20

* Applied load related to the local buckling onset, according with strain gage measurements.

6 Analytical methods for global buckling

In this section, the analytical values of the elastic critical loads for the built-up laced columns are computed according to methods proposed by Timoshenko [12] and Eurocode [21]. The built-up laced columns were considered as pined-pined end condition. As previously reported, the steel properties are *E*=198GPa and 215GPa, respectively for 0.8 and 1.25mm steel plates.

According with Timoshenko [12], the critical load for laced column with "N" lacing, hinged ends and shear effect, is given by Eq. (7):

$$P_{cr} = \frac{\pi^2 EI}{l^2} \frac{1}{1+\frac{\pi^2 EI}{l^2}\left(\frac{1}{A_d\, E\, sen\phi\, cos^2\phi}+\frac{b}{aA_bE}\right)} . \tag{7}$$

where ϕ is the angle between the diagonals and the batten bracings; A_d is the cross-section area of two diagonal members (one at each face of the laced column); A_b is the cross-sectional area of two batten bracings (one at each face of the laced column); b is the length of batten bracings and I is the moment of inertia of the cross-section of the laced column (considering the four chords).

Eurocode EC3 Part 1-3 [6], dedicated to cold-formed steel structures, does not present guidance to the design built-up laced columns. Therefore, Eurocode 3 Part 1-1 [21] design procedure for this type of structural system will be considered. In this condition, the critical load for laced columns is given by Eq. (8):

$$P_{cr} = \frac{\pi^2 EI_{eff}}{L^2} \qquad I_{eff} = 0.5\, A_{ch}\, h_0^2. \tag{8}$$

I_{eff} is the effective moment of inertia of laced built-up members; h_0 is the distance between the centroids of the chords and A_{ch} is the cross-section area of one chord.

Equation (9) gives the effective critical load of built-up column considering shear effect ($P_{cr,v}$):

$$P_{cr,v} = \frac{1}{\frac{1}{P_{cr}}+\frac{1}{S_v}} \qquad S_v = \frac{nEA_d a {h_0}^2}{d^3\left[1+\frac{A_d h_0^3}{A_v d^3}\right]}. \tag{9}$$

S_v is the shear stiffness of built-up columns with "N" lacing arrangement; "n" is the number of lacing plans; A_d is the diagonal cross-sectional area and A_v is the horizontal bracings cross-sectional area, of a single plan; "a" is the length of one panel; "d" is the diagonal length.

Table 12 shows the computed results of the critical flexural buckling loads, for the laced columns, according with the proposed procedures from Timoshenko and Eurocode. Buckling loads from numerical BFEM model and the ratio between critical buckling loads related to BFEM results (inside parenthesis) are also included, from which one may observe quite similar results for both X and Y-axis. These results reveal the analytical method is able to provide accurate results in the present case, as well as the Eurocode procedure gives lower results if compared to analytical solution and numerical BFEM analysis.

Table 12 - Global buckling critical loads: X- axis and Y- axis (kN).

	X - axis			Y - axis		
Column ID	Eurocode	Timoshenko	BFEM	Eurocode	Timoshenko	BFEM
T12x1.25	410 (0.93)	450 (1.02)	442	749 (0.96)	762 (0.98)	777
T12x0.8	243 (0.92)	269 (1.02)	263	444 (0.95)	459 (0.99)	465
T16x1.25	236 (0.93)	260 (1.02)	254	434 (0.95)	445 (0.98)	456
T16x0.8	140 (0.93)	155 (1.03)	151	257 (0.95)	266 (0.99)	270

7 Comparison between BFEM model and experimental collapse loads

The laced column global buckling mode from the numerical buckling analysis was used as the initial geometric imperfection for the BFEM elastic geometrical nonlinear analysis. As recommended in Eurocode 3 part 1-1 [21], the initial geometrical imperfection was adopted as $L/500$. The collapse of the built-up laced columns is recognized when one of the chord members reaches its axial compressive strength. So, the chord members compression forces, obtained from the BFEM elastic non-linear analysis, must be compared with the strength of one chord all along the loading path of the laced column.

Table 13 shows the experimental and numerical collapse loads for the tested built-up laced columns, considering the chord cross-sections with built-up lipped or unlipped channel members from Table 10. It is also included the ratio between numerical and experimental results, inside parenthesis. It is observed that the numerical results for unlipped channel chords presents adequate comparison with the experimental results. These results are sustained by the evidence of collapse mechanism developed at the cross-section with suppression of edge stiffeners. In addition, the last column of Table 13 displays the results of the laced column strength without global buckling effect, taking the axial compression strength of the chords from Table 10 (for built-up unlipped channel option). As expected, this solution gives very much inaccurate comparison with the experimental data.

Table 13: Numerical and experimental collapse loads for the tested built-up laced columns (kN)

Built-up laced column		Experimental	BFEM Non-linear analysis		No global buckling
Column ID	Thickness (mm)	Experimental collapse load	Lipped channel	Unlipped channel	Unlipped channel *
T12x1.25	1.25	233	311 (1.34)	248 (1.06)	359 (1.54)
T12x0.8	0.8	89	152 (1.71)	122 (1.37)	164 (1.84)
T16x1.25	1.25	196	207 (1.05)	186 (0.95)	359 (1.83)
T16x0.8	0.8	85	115 (1.35)	98 (1.15)	164 (1.93)

*See last column of Table 10 for unlipped channel (4 chords).

8 Conclusions

Elastic buckling analysis of steel laced column was performed with analytical and numerical solutions. The obtained results indicated the tested columns perform little influence of the shear effect and the critical buckling load may be accessed with the help of available analytical equations from Eurocode [21] and Timoshenko [12].

As the collapse of the built-up laced columns is recognized when one of the chord members reaches its axial compressive strength, GBTUL and DSM were used to obtain the strength of the built-up CFS chord member. The experimental results for tested chord members indicated marginal influence of the connection between members A and B regarding the column strength, with almost no influence of the number of self-drilling screws. The experimental analysis indicated that the DSM rules are able to estimate the ultimate strength of this type of built-up lipped channel section, adopted

as chords of the laced columns. The better results of the computed chord strength were obtained for the non-composite built-up channel CFS, following experimental evidence of local buckling mode.

Regarding the laced columns, experimental results clearly indicate the presence of global and local buckling during the tests. Large elastic deformation developed before plastic localized collapse at the unlipped channel section (close to diagonal-chord connection).

The tested columns, with nominal length of 12200 and 16200mm, developed important geometric nonlinear behavior from the flexural buckling mode, which was computed with the help of BFEM analysis. The laced column strength was finally computed taking the influence of the local buckling in the chord members, with the help of DSM equations. The obtained results indicate acceptable comparison between computed and experimental data with P_u/P_{uexp} ranging from 0.95 to 1.37 (Table 13). It must be observed that the better results of the computed laced column strength were obtained for the unlipped built-up channel CFS, following experimental evidence of the collapse mechanism developed at these sections.

Acknowledgements

This study was financed in part by the Coordenação de Aperfeiçoamento de Pessoal de Nível Superior- Brasil (CAPES) - Finance Code 001 and the National Council for Research and Technology, CNPq (Process 161975/2015-1). In addition, the authors would like to thank GYPSTEEL Company for the supply of the built-up laced columns and CFS lipped channels, and ARMCO STACO for the supply of the steel end plates.

References

[1] B.H. Hashemi and M.A. Jafari. Experimental evaluation of elastic critical load in batten columns. *Journal of Constructional Steel Research*, 65(1), 125–31, 2009.

[2] A.P. Bonab, B.H. Hashemi and M. Hosseini. Experimental evaluation of the elastic buckling and compressive capacity of laced columns. *Journal of Constructional Steel Research*, 86, 66-73, 2013.

[3] K.E. Kalochairetis, C.J. Gantes and X.A. Lignos. Experimental and numerical investigation of eccentrically loaded laced built-up steel columns. *Journal of Constructional Steel Research*, 101, 66-81, 2014.

[4] B.H. Hashemi and A.P. Bonab. Experimental investigation of the behavior of laced columns under constant axial load and cyclic lateral load. *Engineering Structures*, 57, 536-543, 2013.

[5] M. Dabaon, E. Ellobody and K. Ramzy. Experimental investigation of built-up cold-formed steel section battened columns. *Thin-Walled Structures*, 92, 137–145, 2015.

[6] CEN, EN 1993-1-3:2006. Eurocode 3: Design of steel structures. Part 1-3: General rules, supplementary rules for cold-formed thin gauge members and shetting. *European Committee for Standardization*, Brussels, Belgium, 2006.

[7] AISI, S100-07/S2-10. North American Specification for the Design of Cold-Formed Steel Structural Members. *American iron and Steel Institute*, 2007.

[8] M.A. El Aghoury, A.H. Salem, M.T. Hanna and E.A. Amoush. Experimental investigation for the behavior of battened beam-columns composed of four equal slender angles. *Thin-Walled Structures*, 48 (9), 669–683, 2010.

[9] M.A. Dar, D.R. Sahoo, S. Pulikkal and A.K. Jain. Behaviour of laced built-up cold-formed steel columns: Experimental investigation and numerical validation. Thin-Walled Structures 132 (2018) 398–409, 2018.

[10] F. Engesser. *Die knickfestigkeit gerader stabe* (in german). Zentralbl bauverwaltung, Germany, 1891.

[11] F. Bleich. *Buckling strength of metal structures*. Mcgraw Hill, New York, 1952.

[12] S.P. Timoshenko, J.M. Gere. *Theory of elastic stability*, Mcgraw-Hill, New York, 1963.

[13] Gjelsvik, A., "Stability of built-up columns", ASCE Journal of Engineering Mechanics, 117, 1331-1345, 1991.

[14] M. Paul. Buckling loads for built-up columns with stay plates. *ASCE, Journal of Engineering Mechanics*, 121(11), 1200-1208, 1995.
[15] F. Aslani, S.C. Goel. An analytical criterion for buckling strength of built-up compression members. *Fourth quarter, Engineering Journal, AISC*, 1991.
[16] A.G. Razdolsky. Euler critical force calculation for laced columns. *ASCE Journal of Engineering Mechanics*, 131(10), 997-1003, 2005.
[17] A.G. Razdolsky. Flexural buckling of laced column with serpentine lattice. *The IES Journal part A: Civil & Structural Engineering*, 3(1), 38-49, 2010.
[18] A.G. Razdolsky. Calculation of slenderness ratio for laced columns with serpentine and crosswise lattices. *Journal of Constructional Steel Research*, 67(1), 25–29, 2011.
[19] A.G. Razdolsky. Flexural buckling of laced column with fir-shaped lattice. *Journal of Constructional Steel Research*, 93, 55–61, 2014.
[20] A.G. Razdolsky. Revision of Engesser's approach to the problem of Euler stability for built-up columns with batten plates. *ASCE Journal of Engineering Mechanics*, 140(3), 566-574, 2014.
[21] CEN, EN 1993-1-1:2006 - Eurocode 3: design of steel structures. Part 1-1: general rules and rules for buildings. *European Committee for Standardization*, Brussels, Belgium, 2006.
[22] ABNT, ISO-6892: Materiais metálicos – ensaios de tração a temperatura ambiente. *Associação Brasileira de Normas Técnicas*, Rio de Janeiro, 2013.
[23] B.W. Schafer, T. Peköz. Direct strength prediction of cold-formed steel members using numerical elastic buckling solutions. *In: 14th International Specialty Conference on cold-formed steel structures, St Louis*, Missouri, USA, 69-76, 1998.
[24] ABTN, NBR-14762: Dimensionamento de estruturas de aço constituídas por perfis formados a frio – Procedimento. *Associação Brasileira de Normas Técnicas*, Rio de Janeiro, 2010.
[25] D.C. Fratamico, S. Torabian, X. Zhao, K.J.R. Rassmussen and B.W Schafer. Experimental study on the composite action in sheathed and bare built-up cold-formed steel columns. *Thin-walled Structures*, 127, 290-305, 2018.
[26] X. Liu, T. Zhou. Research on axial compression behavior of cold-formed triple-lambs built-up open T-section columns. *Journal of Constructional Steel Research*, 134, 102-113, 2017.
[27] J.H. Zhang, B. Young. Compression tests of cold-formed steel I-shaped open sections with edge and web stiffeners. *Thin-walled Structures*, 52, 1-11, 2012.
[28] J.H. Zhang, B. Young. Numerical investigation and design of cold-formed steel built-up open section columns with longitudinal stiffeners. *Thin-walled Structures*, 89, 178-191, 2015.
[29] F. Liao, H. Wu, R. Wang and T. Zhou. Compression test and analysis of multi-limbs built-up cold-formed steel stub columns. *Journal of Constructional Steel Research*, 128, 405-415, 2017.
[30] B. Young, J. Chen. Design of cold-formed steel built-up closed sections with intermediate stiffeners. *Journal of Structural Engineering*, 134, 727-737, 2008.
[31] B.W. Schafer, S. Ádány. Buckling analysis of cold-formed steel members using CUFSM: conventional and constrained finite strip methods. *Proceedings of 18th International Specialty Conference on Cold-Formed Steel Structures*, Orlando, 2006.
[32] R. Bebiano, D. Camotim, R. Gonçalves. GBTUL 2.0 – a second-generation code for the GBT-based buckling and vibration analysis of thin-walled members. *Thin-Walled Structures*, 124, 235-253, 2018.
[33] ANSYS R15.0, Inc., *Workbench User's Guide*. Canonsburg: ANSYS, Inc., 2015.
[34] G.Y. Matsubara, E.M. Batista, G.C. Salles. Lipped channel cold-formed steel columns under local-distortional buckling mode interaction. *Thin-walled Structures*, 137, 251-270, 2019.
[35] SAP 2000 Version 15. Getting Started with SAP 2000 Linear and Nonlinear Static and Dynamic Analysis and Design of Three-Dimensional Structures. *Computers and Structures Inc.* Berkeley, California, USA, Abril, 2011.